α-CGRP Disrupts Amylin Fibrillization and Regulates Insulin Secretion: Implications on Diabetes and Migraine

Amber L. H. Gray,[a,‡] Aleksandra Antevska,[a,‡] Benjamin A. Link,[a,†] Bryan Bogin,[b,c], Susan J. Burke,[d] Samuel D. Dupuy,[f] J. Jason Collier,[e] Zachary A. Levine,[b,c] Michael D. Karlstad,[f] Thanh D. Do[a,*]

[a] Department of Chemistry, University of Tennessee, Knoxville, TN 37996

[b] Laboratory of Islet Biology and Inflammation, Pennington Biomedical Research Center, Baton Rouge, LA 70808

[c] Department of Surgery, Graduate School of Medicine, University of Tennessee Health Science Center, Knoxville, TN 37920

[d] Department of Pathology, Yale School of Medicine, New Haven, CT 06520

[e] Department of Molecular Biophysics & Biochemistry, Yale University, New Haven, CT 06520

SUPPORTING INFORMATION

Table of Contents

Transmission Electron Microscopy Procedure

The staining process was performed on a small piece of parafilm. A drop of sample, distilled water, and 1% phosphotungstic acid stain were placed onto the parafilm. A copper grid with thin carbon film was floated on the drop of sample, film side down. After 90 seconds, the grid was removed from the sample drop and excess sample was removed by touching the edge of the grid to a piece of Whatman filter paper. The grid was immediately touched to a drop of disttiled water for 1 second, the water removed, and the grid, film side down, was placed on a drop of 1% phosphotungstic acid stain. After 60 seconds, the grid was removed from the stain and quickly dried by touching the edge of the grid to a piece of filter paper. After drying, the grid with sample was imaged on a JEOL 1400 Flash transmission electron microscope operating at 80kV. Images were recorded with a Gatan OneView camera.

S1. Supporting Tables

Table S1. Agilent 6560 IMS-QTOF Parameters

The pressure of the drift tube is 3.940 Torr with the pressure differences between the drift tube and trap funnel being approximately 300 mTorr.

	Parameter	Value
Pre-IMS Zone	Source: Gas Temperature	300 ^{o}C
	Source: Drying Gas	5 L/min
	Source: Nebulizer Pressure	13 psi
	Source: Capillary	3800 V
	Optics I: Fragmentor	250 V
	IM Front Funnel: High Pressure Funnel Delta	110 V
	IM Front Funnel: High Pressure RF Delta	180 V
	IM Front Funnel: Trap Funnel Delta	160 V
	IM Front Funnel: Trap Funnel RF	180 V
	IM Front Funnel: Trap Funnel Exit	10 V
	IM Trap: Trap Entrance Grid Low	82 V
	IM Trap: Trap Entrance Grid Delta	2 V
	IM Trap: Trap Entance	79 V
	IM Trap: Trap Exit	76 V
	IM Trap: Trap Exit Grid 1 Low	72 V
	IM Trap: Trap Exit Grid 1 Delta	6 V
	IM Trap: Trap Exit Grid 2 Low	71 V
	IM Trap: Trap Exit Grid 2 Delta	13 V
	Acquisition: Trap Fill Time	1000 µs
	Acquisition: Trap Release Time	100 µs
Post-IMS Zone	IM Drift Tube: Drift Tube Exit	210 V
	IM Rear Funnel: Rear Funnel Entance	200 V
	IM Rear Funnel: Rear Funnel RF	130 V
	IM Rear Funnel: Rear Funnel Exit	35 V
	IM Rear Funnel: IM Hex Entrance	42 V
	IM Rear Funnel: IM Hex Delta	-8
	Optics 1: Oct Entrance Lens	32 V
	Optics 1: Lens 1	28.3 V
	Optics 1: Lens 2	15.8 V
	Quad: Quad DC	26.6 V
	Quad: Postfilter DC	26.5 V
	Cell: Gas Flow	22 psi
	Cell: Cell Entrance	25.6 V
	Cell: Hex DC	24.2 V
	Cell: Hex Delta	-9 V
	Cell: Hex2 DC	15 V
	Cell: Hex2 DV	-3 V
	Optics 2: Hex3 DC	11.8 V
	Extractor: Ion Focus	5.6 V

Table S2. Collisional cross sections of Ins1 monomers in N_2 and He

z	*m/z*	CCS_{N2} (Å^2)	CCS_{He} (Å^2)[†]	CCS_{He} (Å^2)[1]
+7	829.655	1323	1121	-
		1411	1199	-
+6	967.751	1181	997	-
		1237	1047	-
+5	1161.084	1389	1180	-
		1134	956	-
+4	1450.804	936	783	772
		902	753	-

[†]The collisional cross sections of Ins1 were obtained in N_2 and then calibrated to He values.

[1] Salvo et al. (2012). The literature value is for human insulin.

S2. Supporting Figures

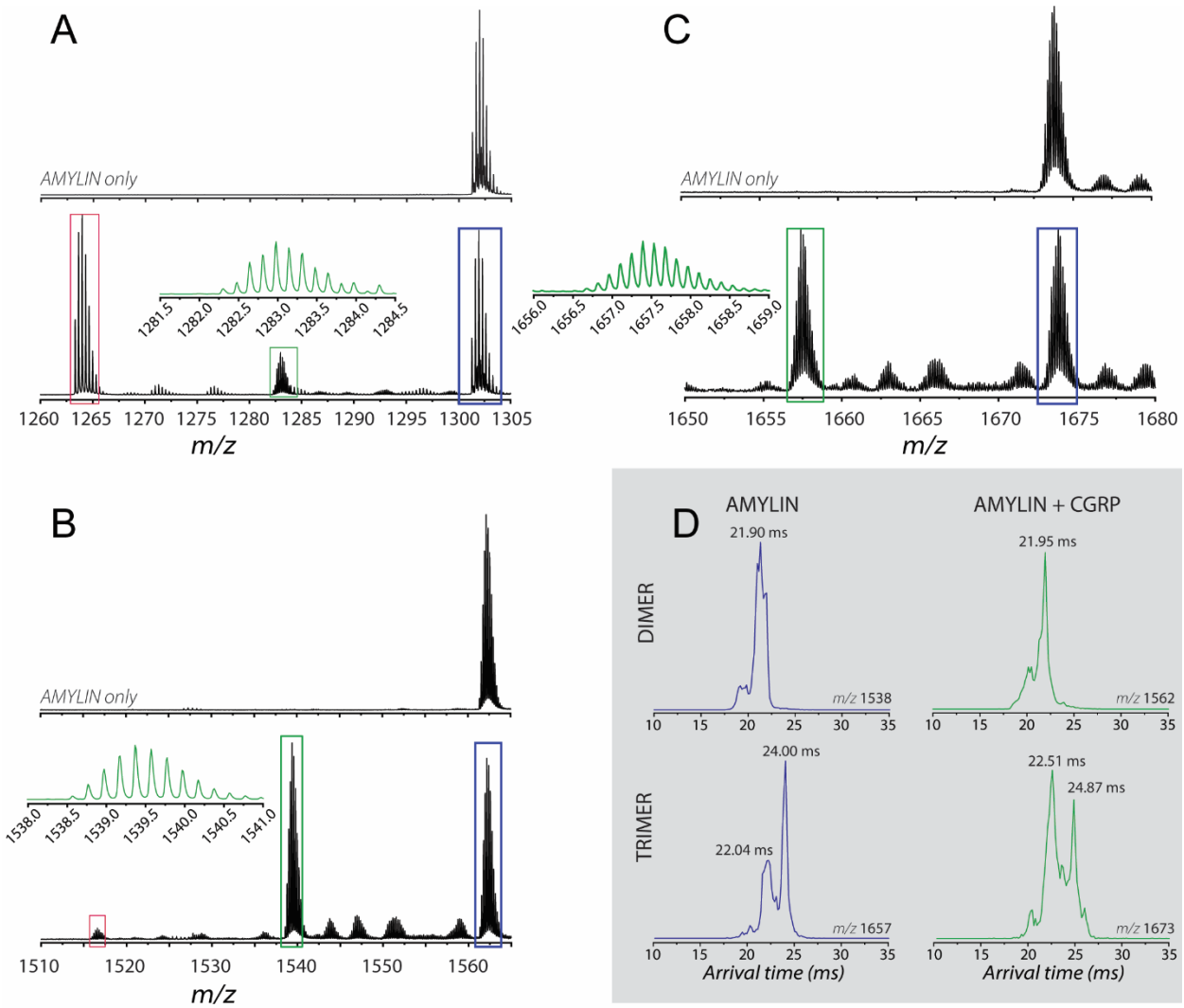

Figure S1. Partial mass spectra of amylin:CGRP hetero- dimer and trimer and corresponding ATDs. For panels A – C, the top mass spectrum is of amylin alone and the bottom mass spectrum is of the amylin:CGRP mixture. Within the partial mass spectra, the mass spectral peaks boxed in blue correlate to amylin, red is CGRP, and green represents co-oligomeric species. (A - B) amylin:CGRP (1:1) heterodimers (C) amylin:CGRP (2:1) heterotrimer (D) ATDs of amylin dimer and trimer (left) and amylin:CGRP hetero- dimer and trimer (right).

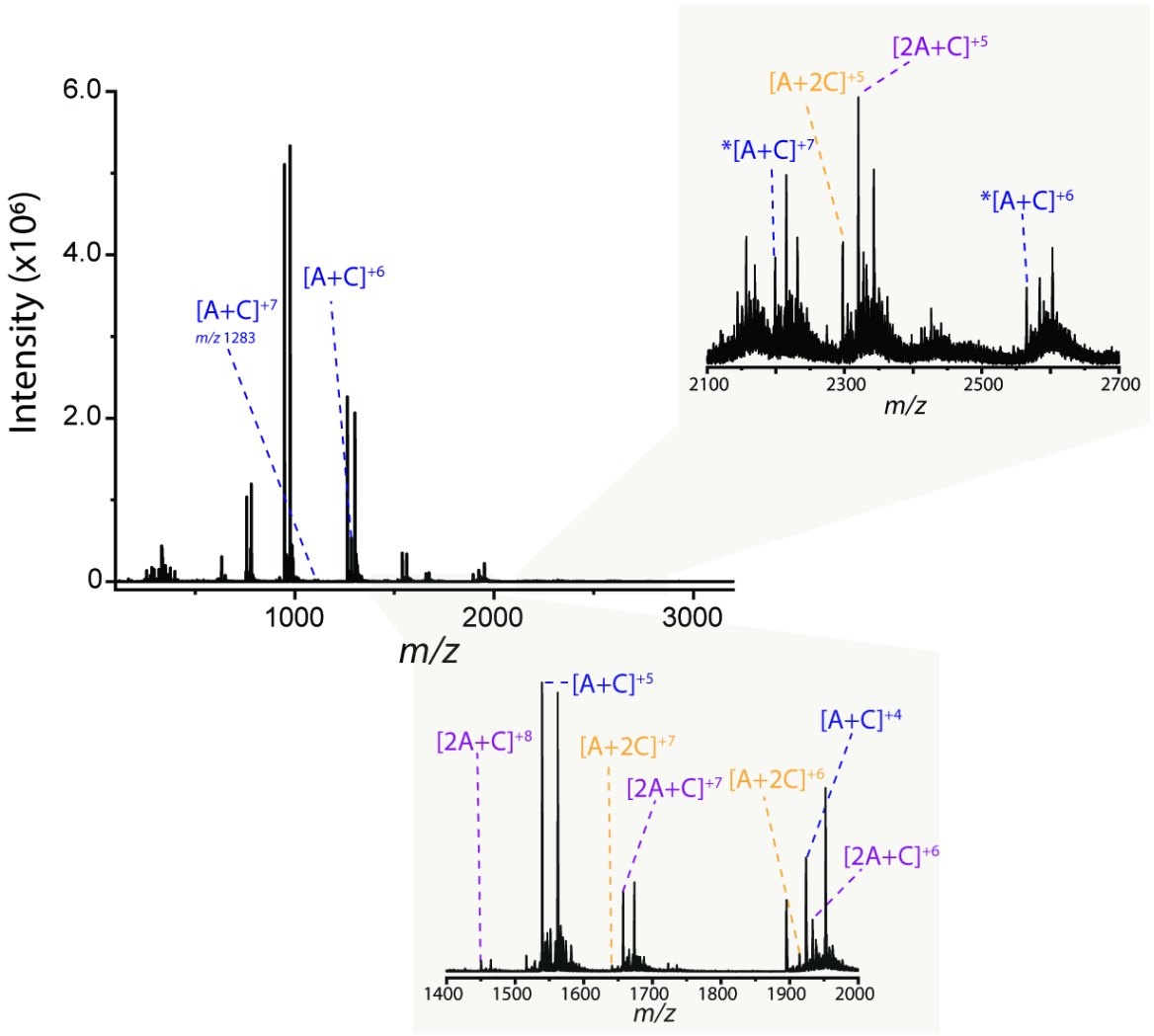

Figure S2. Representative mass spectrum of amylin:CGRP.

The mass spectrum of 1:1 amylin:CGRP (5:5 µM) in 20 mM ammonium acetate at *t* = 0. Mass spectral peaks labeled "A+C" represents oligomers composed of 1:1 amylin:CGRP, "2A+C" represents oligomers made up of 2:1 amylin:CGRP, and "A+2C" represents oligomers of 1:2 amylin:CGRP. Note the asterisk next to the 1:1 amylin:CGRP species at *z = +7* and *+8* in the 2100 – 2700 mass range. These are species that are composed of 2:2 amylin:CGRP.

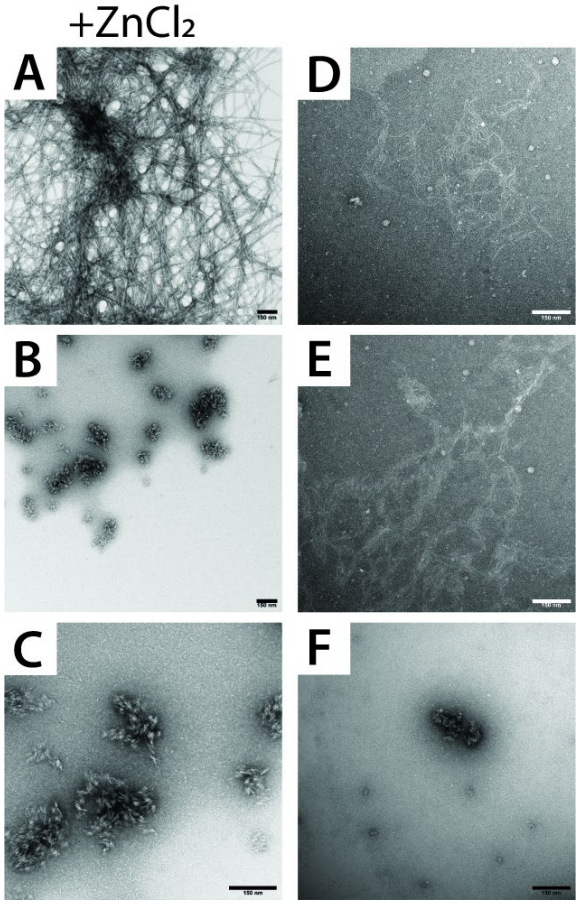

Figure S3. TEM images of amylin:CGRP with and without $ZnCl_2$.

Representative TEM images of the amylin:CGRP mixture with Zn and without Zn. The samples with Zn had a mixture of material, including (A) long fibrils and (B-C) short fibrils. The short fibrils look similar in morphology to the globular aggregates (e.g. panel F). The samples without Zn primarily exhibited globular aggregates, however there were some faint and indistinct fibrillar species present (D-E). The scale bar is a 150 nm.

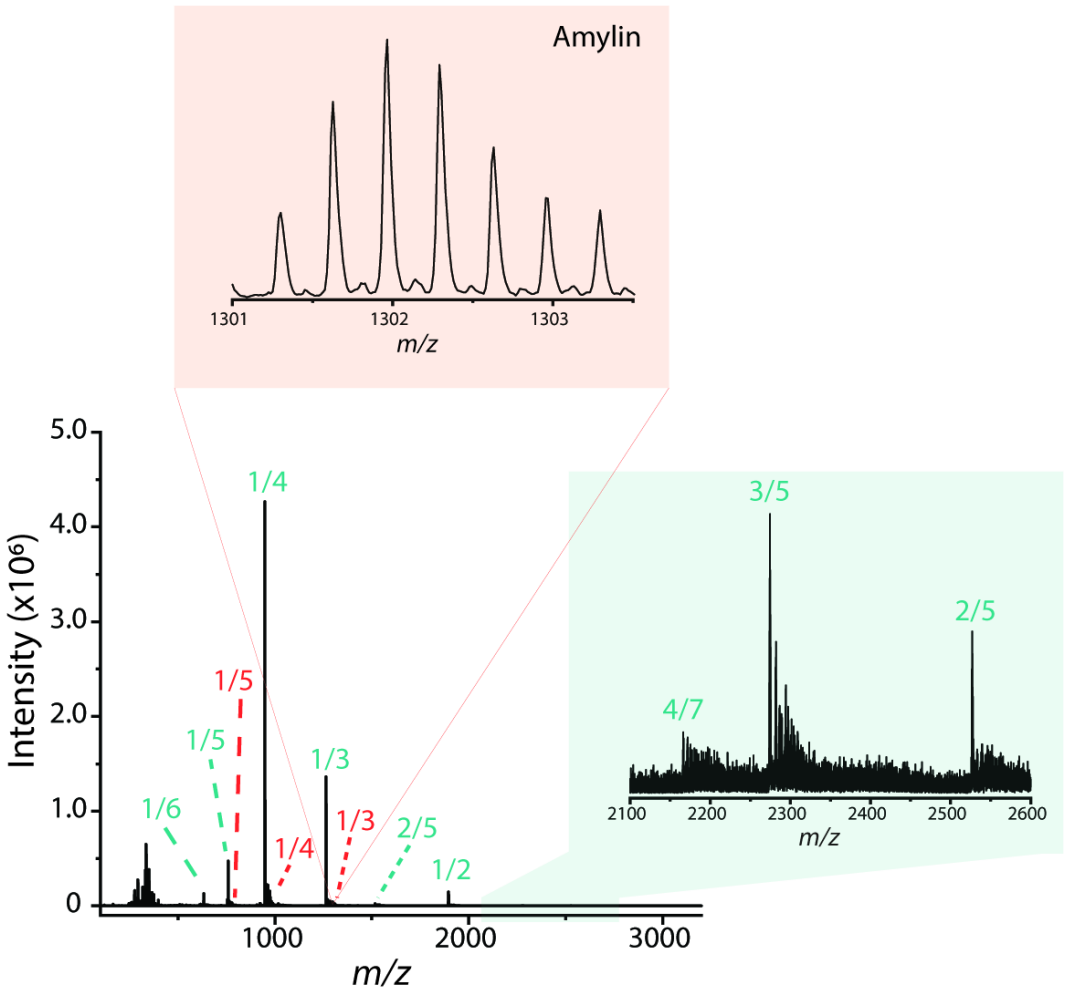

Figure S4. Representative mass spectrum of amylin:CGRP after one week.

The mass spectrum of 1:1 amylin:CGRP (5:5 µM) in 20 mM ammonium acetate after setting out at room temperature for one week. Only peaks corresponding to CGRP (blue) and amylin (orange) are labeled. Note that the intensity of the amylin peaks are much lower than what is shown in Figure S2. This implies that amylin has fell out of solution to form globular aggregates.

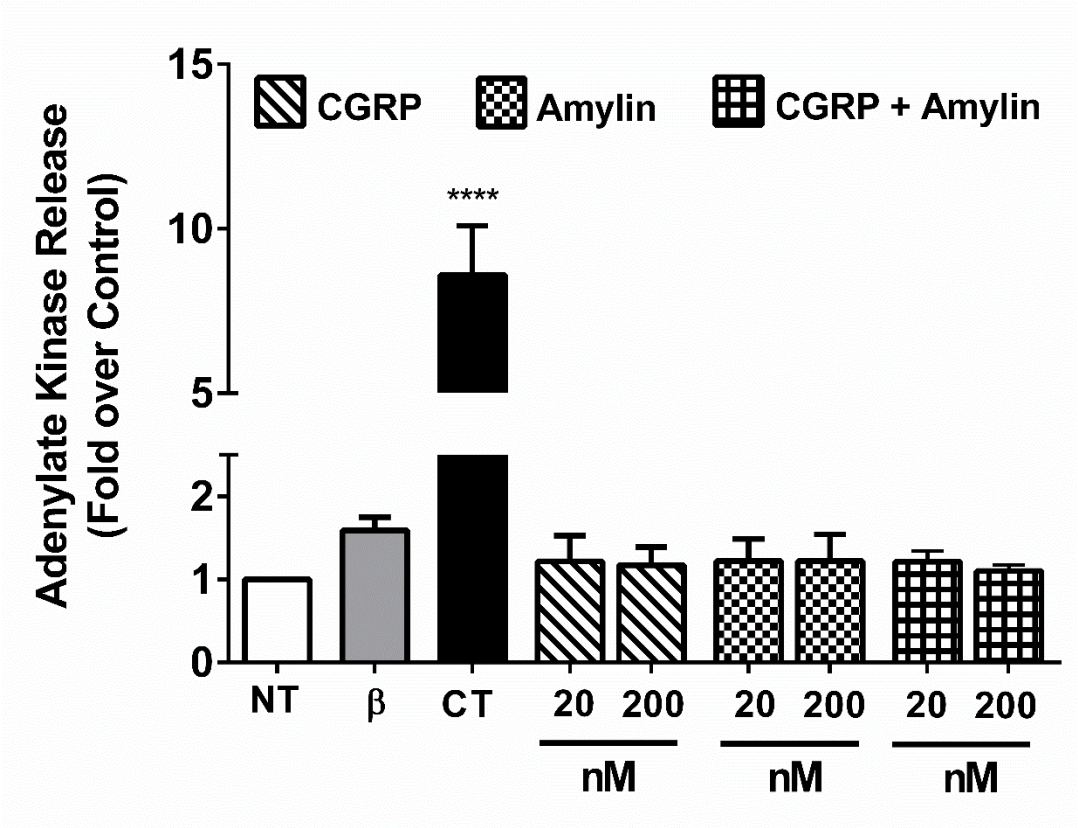

Figure S5. Cell viability assay using cultured β-cells.

Cell viability assay using cultured β-cells exposed to CGRP, amylin, and amylin:CGRP. 832/13 rat b-cells were either left untreated (NT) or exposed to 1 ng/mL IL-1b, 2 mM camptothecin (CT) compared with 20 and 200 nM of amylin, CGRP, or amylin plus CGRP for 18 h. ****, $p < 0.0001$ versus NT using one-way ANOVA. n = 4-6 per group. When compared to CT, there effects of amylin, CGRP, or amylin+CGRP on cellular viability are minor, although amylin has a stronger effect than other two conditions.

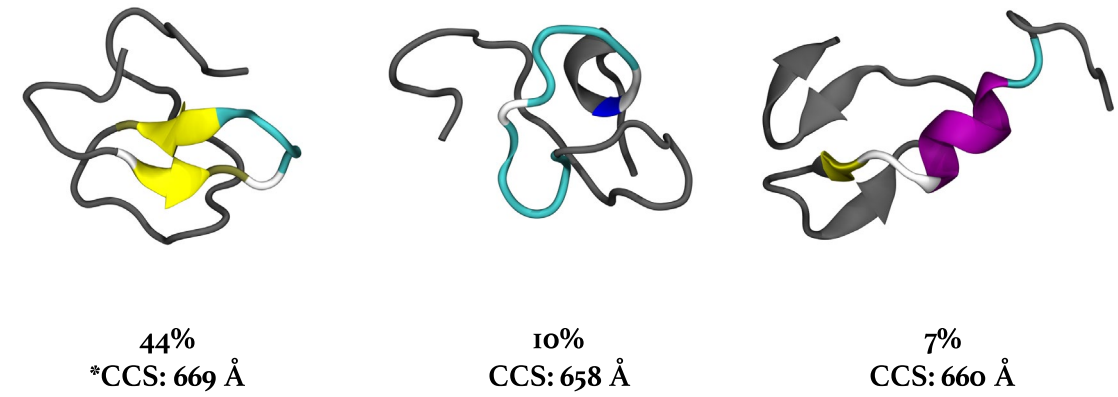

Figure S6. Representative structures of CGRP monomers obtained from REMD simulations and clustered together by residues 8-18.

CCS values for these eigenstates are in excellent agreement with IM-MS data.

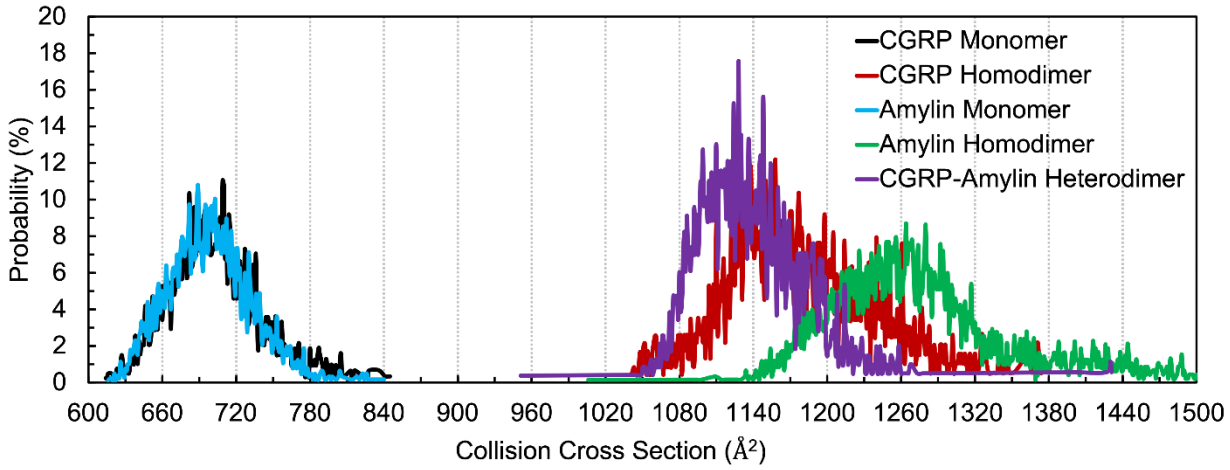

Figure S7. CGRP and amylin CCS from REMD simulations reveal small disordered CGRP-containing homodimers and heterodimer compared to larger β-stranded amylin dimers.

Theoretical CCS distributions from simulations containing CGRP or amylin monomers, homodimers, and heterodimers are displayed in Figure S7. Broadly, the distribution of monomeric cross sections between CGRP and amylin (black and blue, respectively) are quite similar, and sample cross sections that overlap with the experimental data (623-724 Å^2). However, unlike experiments, there is only a single peak for each monomer, though the difference in solvents between simulations and mass spec is likely to introduce discrepancies between these measurements. Notably, though, the monomeric peaks from MD agree with the experimental CGRP peak and the midpoint between experimental amylin peaks. During dimerization, amylin homodimers (green) form extended β-strands that are typical of amyloid fibrils while CGRP homodimers (red) adopt a disordered conformation with a smaller cross section.

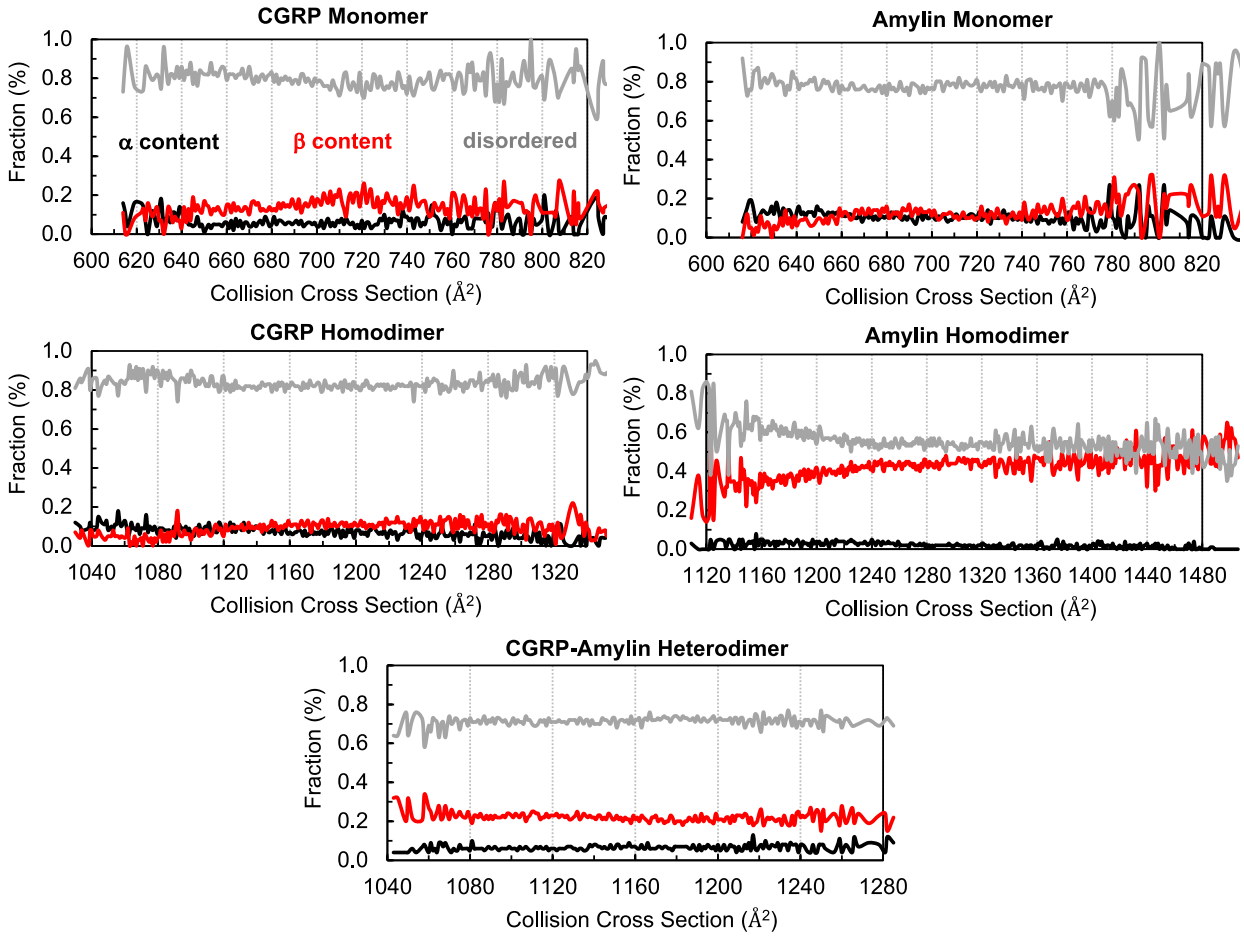

Figure S8. Theoretical CCS values as a function of corresponding protein secondary structures from REMD, which highlight significantly disordered conformations.

For each state sampled in REMD, a corresponding CCS was calculated using the MOBCAL package. Conformations with similar CCS values were binned and averaged together. These measurements highlight that a-helical fractions tend to correspond to lower CCS values while b-stranded conformations tend to correspond to higher CCS values. Similarly, the ability of REMD to sample intermediate states that capture a wide range of protein conformations highlights it's usefulness as an index to interpret IMS-MS data.

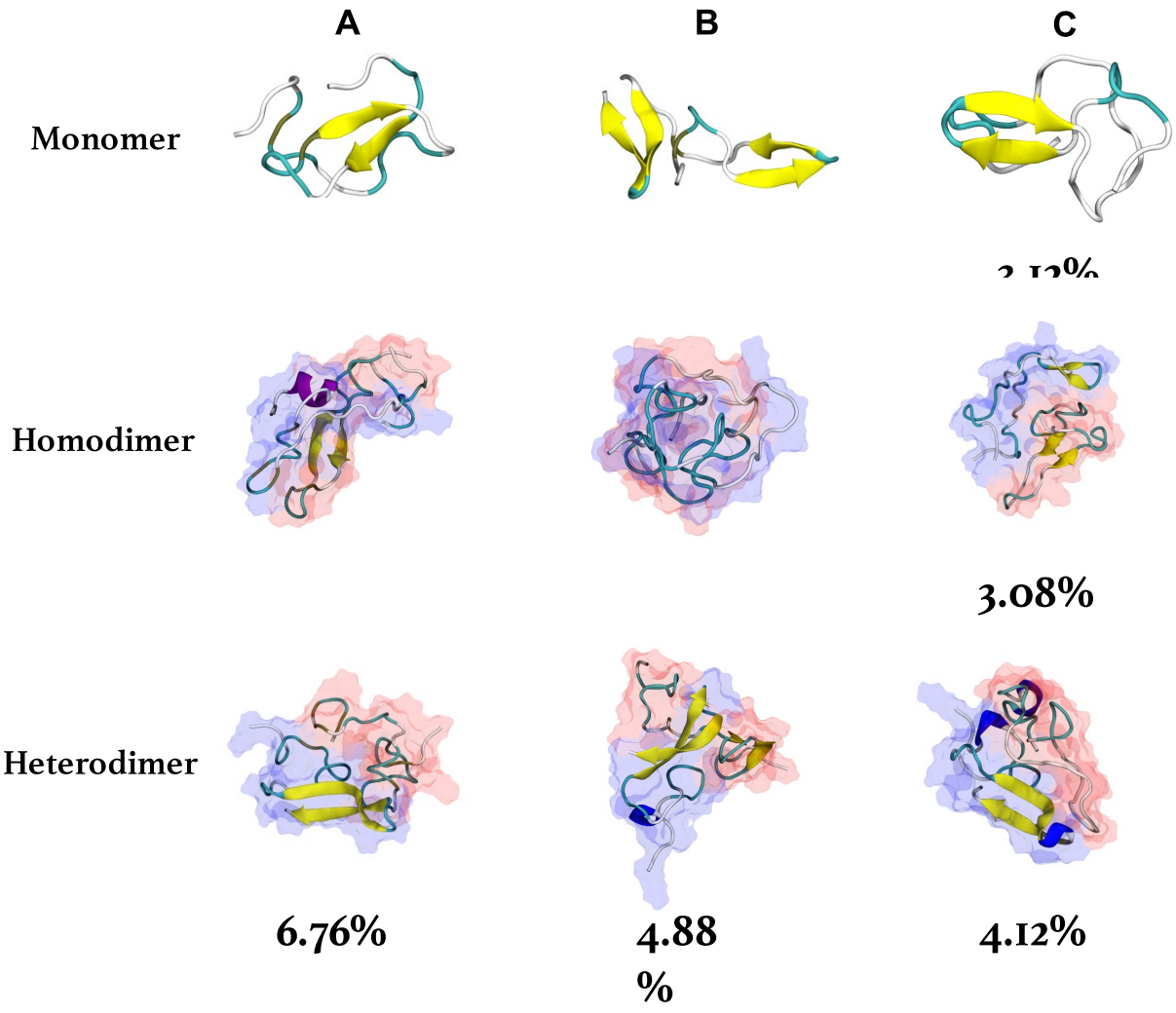

Figure S9. Representative structures of CGRP monomers (*top*), homodimers (*middle*), and heterodimers (*bottom*) obtained from REMD simulations.

Clusters A, B, and C indicate representative eigenstates that are populated in various amounts throughout the simulations, though a large proportion of states are disordered and do not contribute to well-defined secondary structures.

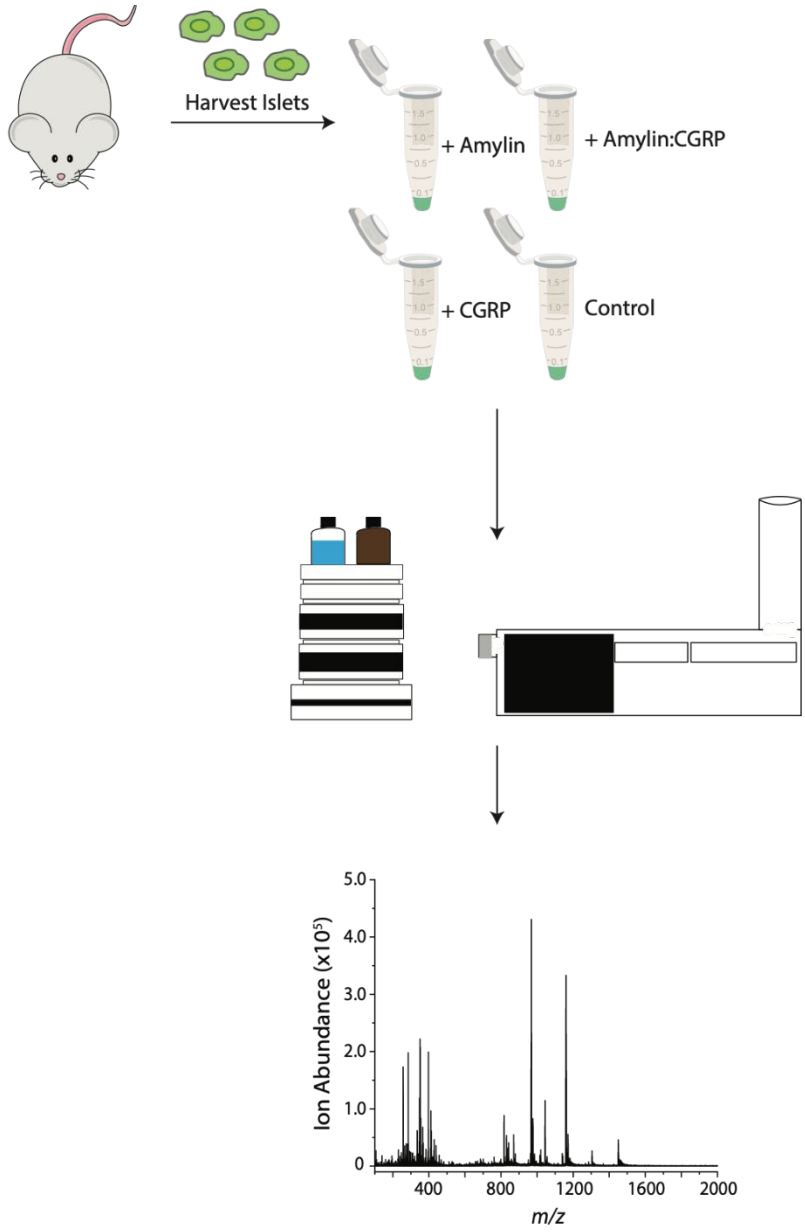

Figure S10. Schematic of single islet analysis workflow.

The workflow for the single islet analysis. Briefly, pancreatic islets from a mouse were isolated and placed into an Eppendorf tube which contained media (control) or media spiked with either amylin, amylin:CGRP, or CGRP. The islets were then analyzed via LC-IMS-MS.

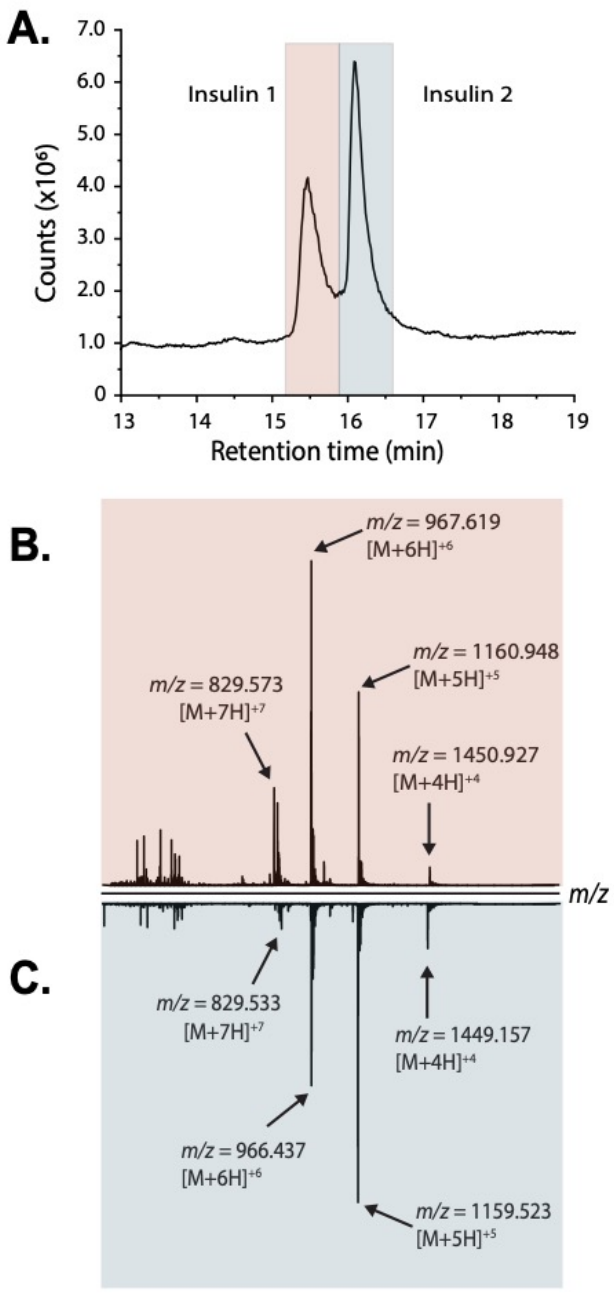

Figure S11. Extracted LC chromatogram of Ins1 and Ins2. Extracted partial LC-MS mass spectrum of Ins1 and Ins2.

Both Ins1 and Ins2 were detected upon LC-IMS-MS analysis (A). Ins1 was detected at four different charge states (B). The species at *m/z* 967.619 is the most intense, and other charge states were at *m/z* 829.963 (*z* = +7), 1060.943 (*z* = +5), and 1451.182 (*z* = +4). Ins2 was detected at four different charge states (C) which were identified unambiguously with isotopic spacings. The $[M+5H]^{5+}$ species at 1159.523 is the most intense and other charge states were at *m/z* 829.533 (*z* = +7), 966.437 (*z* = +6), and 1449.157 (*z* = +4).

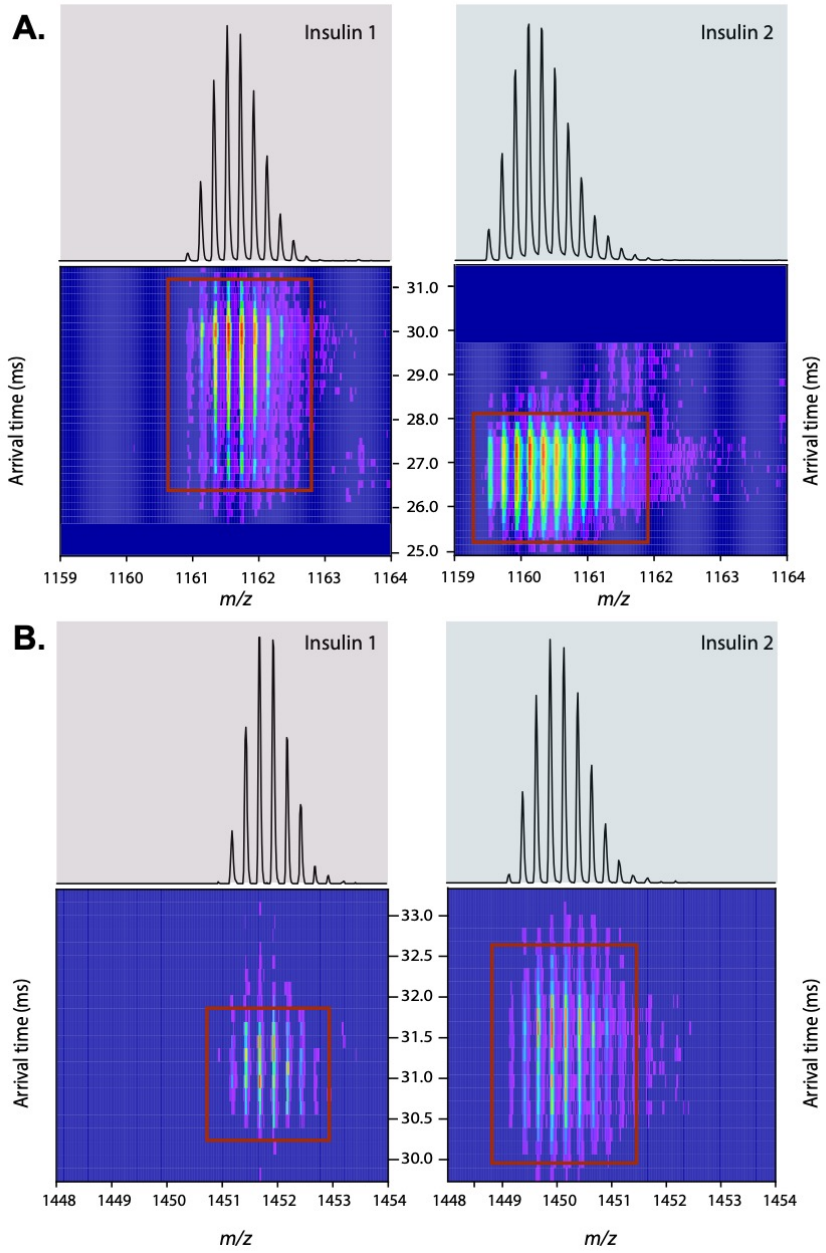

Figure S12. 2D plots of *m/z* vs. arrival time of Ins1 and Ins2 at z = +5 (A) and z = +4 (B)

The 2D plots of arrival time vs. *m/z* show the structural difference between Ins1 and Ins2. The arrival time of Ins2 at ~26-27 ms corresponds to the suggestion that Ins2 either adopts a more compact conformation or it is more prone to form oligomers.

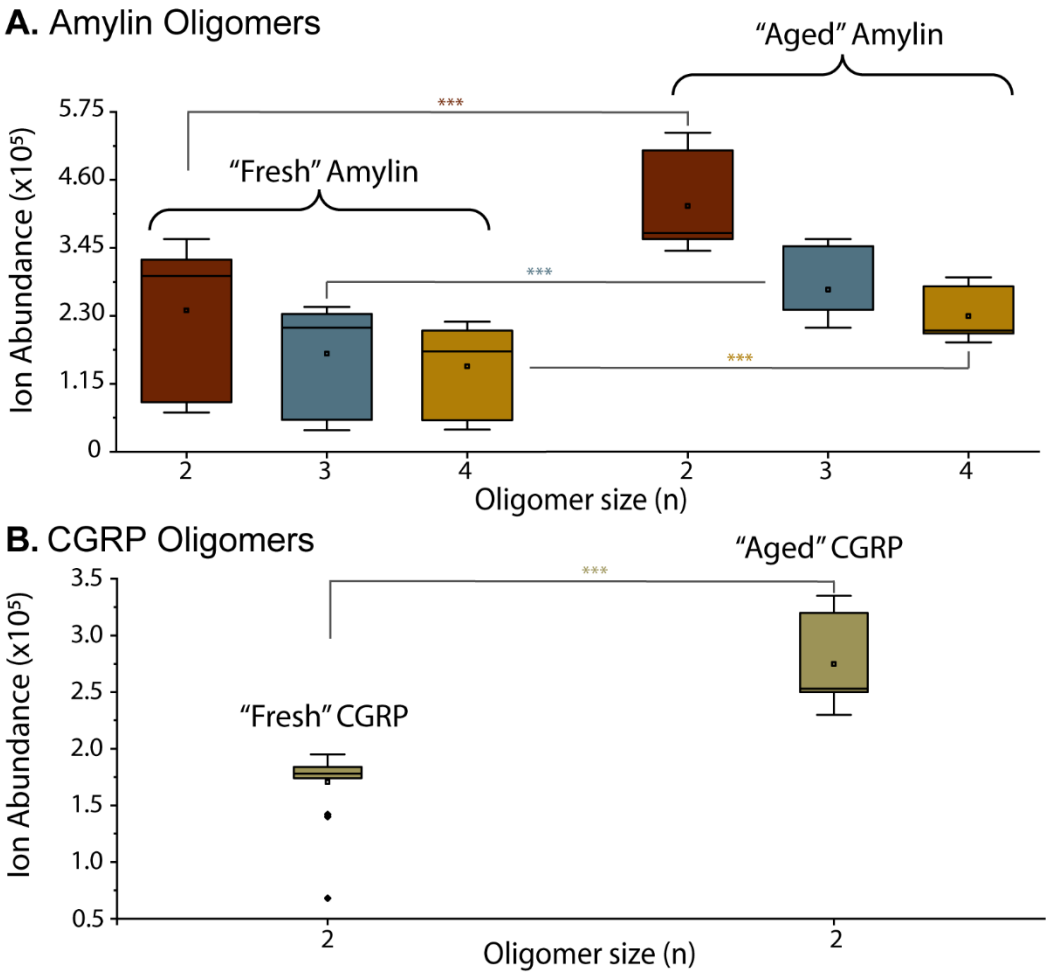

Figure S13. Comparisons of amylin and CGRP oligomers in "fresh" and "aged" incubating solutions.

Amylin oligomers up to tetramers were detected, whereas CGRP oligomers up to dimers were detected in the two different solutions. The ion abundance of the oligomers increased in the aged peptides solutions. A paired t-test was performed to check for variation between the oligomers in the different solutions. *** indicates significant difference.

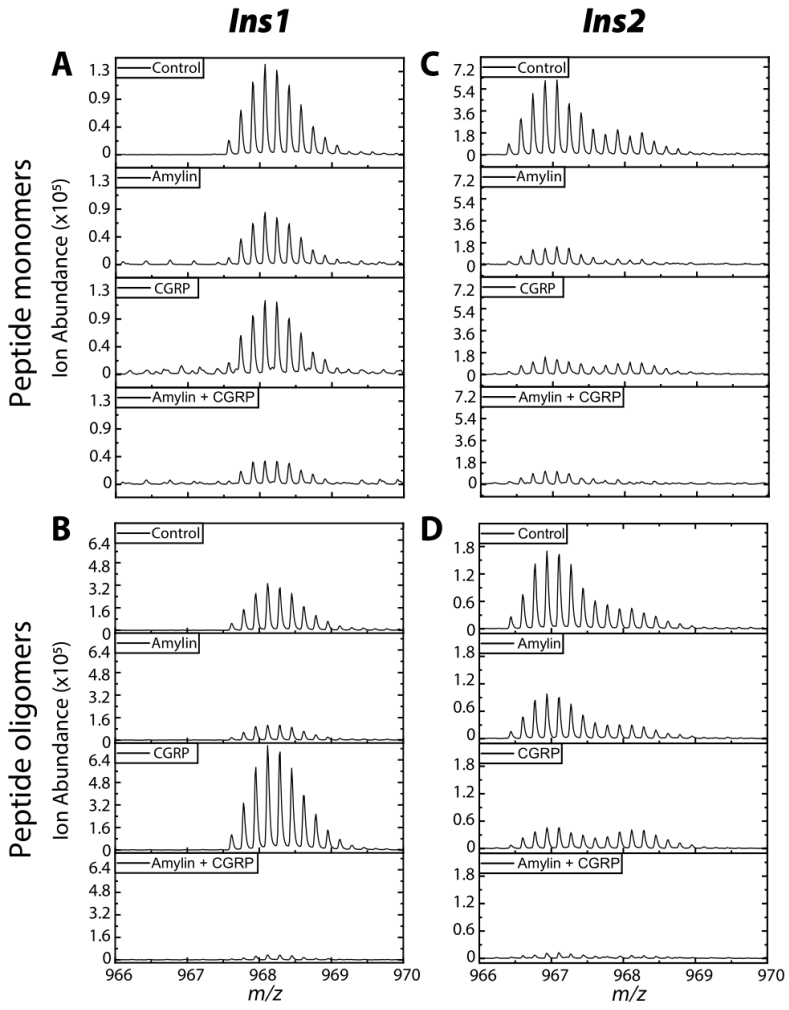

Figure S14. Raw abundances of insulin in incubating solutions containing peptide monomers *vs.* peptide oligomers.

Comparisons of raw insulin signals obtained from single islets exposed to (A, C) “fresh” peptide solution (i.e. peptide monomers) and (B, D) “aged” peptide solution (i.e. peptide oligomers).

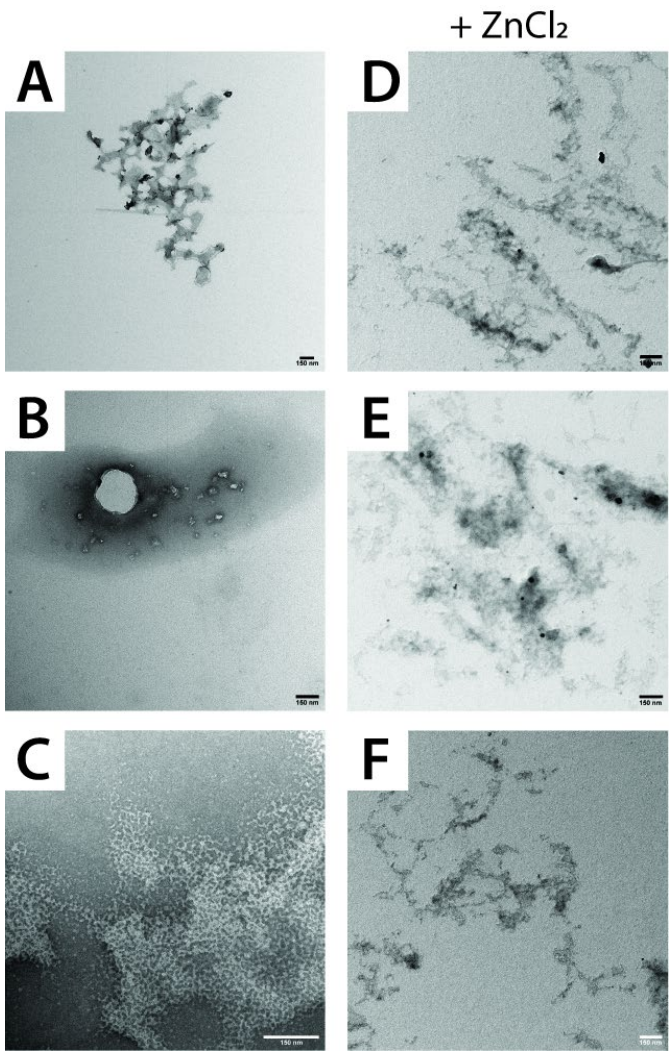

Figure S15. TEM images of CGRP with and without Zinc.

TEM images of CGRP at a larger FOV with and without Zinc. Note that species depicted in each TEM image is believed to be artifacts or random debris. Scale bar is 150 nm.

References Cited

(1) Salbo, R.; Bush, M. F.; Naver, H.; Campuzano, I.; Robinson, C. V.; Pettersson, I.; Jorgensen, T. J.; Haselmann, K. F., Traveling-wave ion mobility mass spectrometry of protein complexes: accurate calibrated collision cross-sections of human insulin oligomers. *Rapid Commun. Mass Spectrom.* **2012**, 26 (10), 1181-93.

(2) Levine, Z. A.; Teranishi, K.; Okada, A. K.; Langen, R.; Shea, J.-E. The Mitochondrial Peptide Humanin Targets but Does Not Denature Amyloid Oligomers in Type II Diabetes. *J. Am. Chem. Soc.* **2019**, *141* (36), 14168–14179. https://doi.org/10.1021/jacs.9b04995.